Synchronization of Van der Pol oscillators in a thermal bath

Dixian Ruan ,[1] Junjie Liu ,[2,*] and Changqin Wu [1,†]
[1]*Department of Physics and State Key Laboratory of Surface Physics, Fudan University, Shanghai 200433, China*
[2]*Department of Physics, International Center of Quantum and Molecular Structures, Shanghai University, Shanghai 200444, China*

(Received 15 January 2023; accepted 7 July 2023; published 7 August 2023)

The phenomenon of synchronization in self-sustained systems has been successfully illuminated in many fields, ranging from biology to electrical engineering. To date, the majority of theoretical studies on synchronization focus on isolated self-sustained systems, leaving the effects of surrounding environments less touched due to the lack of appropriate descriptions. Here we derive a generalized Langevin equation that governs the dynamics of open classical Van der Pol (VdP) oscillators immersed in a common thermal bath with arbitrary memory time and subsumes an existing equation for memoryless bath as a special limit. The so-obtained Langevin equation reveals that the bath can induce a dissipative coupling between VdP oscillators, besides the usual damping and thermal noise terms connected by the fluctuation-dissipation theorem. To demonstrate the utility of the approach, we investigate a model system consisting of two open VdP oscillators coupled to a thermal bath with an Ohmic or a Lorentzian-shape spectrum. Unlike the isolated setup where the stable synchronization can be either in-phase or antiphase when varying initial conditions, we find that the bath always favors a single type of synchronization in the long-time limit regardless of initial conditions and the synchronization type can be switched by tuning the temperature. Moreover, we show that the bath-induced dissipative coupling can trigger a synchronization of open VdP oscillators that is otherwise absent between isolated counterparts. Our results complement and extend previous findings for open VdP oscillators.

DOI: 10.1103/PhysRevE.108.024207

I. INTRODUCTION

The synchronization phenomenon was first observed and studied by the physicist Huygens in the 17th century on two pendulum clocks under an identical support beam [1]. Much progress has been made on this topic in the last 20 years. Now it has become one of the most compelling topics through a wide range of physical frontier areas, from nonlinear dynamical mechanics [2–5] to modern quantum systems such as trapped ions [6] and optomechanical nanodevices [7–9]. Synchronization generally occurs in self-sustained systems such as aforementioned pendulum clocks and metronomes whose dynamics is essentially nonlinear; among them the Van der Pol (referred as VdP) oscillator is one of the representative models [10]. It is generally recognized that synchronization manifests as an adjustment of rhythms between oscillators. This adjustment can occur when two self-sustained oscillators [11,12] or a large ensemble of oscillators [13–15] experience weak interactions between them [2,16,17] or by simply responding to a periodic external driving force [18]. Synchronization finds applications in many aspects such as automatic controlling [19,20], physiology research, or bio-inspired systems [21].

In recent years, researchers have started to investigate synchronization of open self-sustained oscillators subject to external noise induced by their surrounding baths. Prototypical studies have been carried out in excitable systems [22], for instance, Van der Pol–Duffing systems [23], bistable Kramers oscillators [18,24–26], FitzHugh-Nagumo excited systems stemmed from simple VdP oscillators [27,28], chaotic Rössler oscillators [29], and an arbitrary dynamical system in a stable limit cycle [30]. These studies have uncovered multiple effects of baths on synchronization. For example, once the fixed elastic beam in the Huygens experiment is perturbed by external noise, a noise-induced in-phase synchronization as opposed to the original antiphase one would occur [31]. These findings have played a crucial role in many applications such as vertical-cavity lasers [32], optical tweezers [33], VdP circuits [19], or biological systems [34].

Despite the aforementioned progress, synchronization in open self-sustained oscillator systems still warrants further investigations, especially noting that there is still no well-accepted way of incorporating effects of thermal baths into otherwise self-sustained oscillators. Conventionally, one just directly modifies the equation of motion (EOM) for self-sustained oscillators by adding a noise term and a damping term in a phenomenologically manner. For instance, in [27,35], the authors proposed the following generalized EOM for an open VdP oscillator with coordinate x:

$$\ddot{x} + \gamma\dot{x} + \omega^2 x + ax^2\dot{x} = \xi(t). \tag{1}$$

Here $\ddot{x}$ ($\dot{x}$) marks the second- (first-) order time derivative, ξ denotes a white noise term with a correlation function $\langle\xi(t)\xi(t')\rangle = 2D\delta(t-t')$, D quantifies the noise intensity, and ω and a are the oscillator frequency and strength of nonlinearity, respectively. We remark that the damping strength $\gamma = \gamma_{\rm in} + \gamma_{\rm ext}$ contains two contributions: intrinsic

*jj_liu@shu.edu.cn
†cqw@fudan.edu.cn

component $\gamma_{\rm in}$ persisting in isolated VdP oscillators and the external component $\gamma_{\rm ext}$ induced by the bath. While it is straightforward to cast these two contributions into a single parameter γ in the white noise case, this simplification is no longer applicable when considering thermal baths that can generate colored noise as the corresponding damping strength $\gamma_{\rm ext}$ becomes explicitly time-dependent [36,37]; see also Eq. (6) below. Moreover, Eq. (1) does not impose the connection between D and $\gamma_{\rm ext}$ as guaranteed by the fluctuation-dissipation theorem.

Here we aim to obtain a generalized EOM for open VdP oscillators that could enable the inclusion of thermal baths of arbitrary memory time thereby gaining a deeper understanding of synchronization of open VdP oscillators. To this end, we treat the bath and system-bath coupling in terms of Hamiltonians in light of the Caldeira-Leggett model [38], and combine the resulting EOMs from the Hamiltonians for bath and system coordinates with the inherent one for the isolated VdP oscillators [10] that cannot be derived from a Hamiltonian. By doing so, we can obtain a generalized Langevin-type EOM [cf. Eq. (6)] that is similar to Eq. (1) but enables the description of colored noise. From the resulting EOM, we find that the common bath generally affects VdP oscillators in two ways: (1) establishing a dissipative interaction between oscillators [3] and (2) inducing a random thermal motion by generating a random thermal noise whose variance is explicitly connected to an external damping via the fluctuation-dissipation theorem.

To demonstrate the utility of the so-obtained generalized EOM, we consider two coupled VdP oscillators [10] immersed in a thermal bath whose spectral function is chosen to be of an Ohmic or a Lorentzian type, thereby generating a white or colored noise term, respectively. We show that the bath-induced dissipative coupling can induce synchronization of open VdP oscillators [cf. Figs. 6(b) and 9(b)] that is otherwise absent when considering isolated counterparts. We also find that the bath favors a single type of synchronization among in-phase and antiphase ones regardless of initial conditions, in stark contrast to the isolated scenario in which the synchronization type is sensitive to initial conditions. Particularly, for the EOMs [cf. Eqs. (15) and (16)] we considered, we show that a relatively low-temperature bath stabilizes an in-phase synchronization [cf. Figs. 4(c) and 11(a) for white and colored noise, respectively], while a relatively high-temperature bath can instead select an antiphase synchronization [cf. Figs. 5(b) and 11(b) for white and colored noise, respectively]. We attribute this bath-induced synchronization selection phenomenon to the distinct roles of bath-induced dissipative coupling and the noise term in shaping the dynamics. At low temperatures, the bath-induced dissipative coupling dominates, and it can induce an in-phase synchronization as noted by Refs. [3,39,40], while in the high-temperature regime, the noise term plays a major role. The sign difference between the noise terms that appears in EOMs [cf. Eqs. (15) and (16)] forces the two oscillators to synchronize in an antiphase way. We complement this picture by showing in Appendix A that a high-temperature bath can stabilize an in-phase synchronization [cf. Fig. 12(c)] when the signs of the noise terms in EOMs [cf. Eqs. (B3) and (B4)] are the same.

The paper is organized as follows. In Sec. II we first derive a generalized EOM for open VdP oscillators, then introduce a model system consisting of two VdP oscillators coupled to a bath. In Sec. III we consider a bath with an Ohmic spectrum and analyze in detail the effects of white noise on synchronization behavior. In Sec. IV we turn to a bath with a Lorentzian-shape spectrum and address the effects of colored noise. We summarize the study in Sec. V.

II. OPEN VAN DEL POL OSCILLATORS

A. Generalized equation of motion

We consider N coupled open VdP oscillators with coordinates $\{x_1, x_2, \dots, x_N\}$ placed in a bath and aim to derive a generalized EOM governing the dynamics of those coordinates. We model the bath and the system-bath coupling in terms of the following Hamiltonians [38]:

$$H = H_B + H_C = \sum_j \left(\frac{p_j^2}{2m_j} + \frac{1}{2} m_j \nu_j^2 q_j^2 \right) + \sum_{i,j} C_{ij} x_i q_j. \tag{2}$$

Here the thermal bath is represented by an ensemble of harmonic oscillators with masses m_j, frequencies ν_j, coordinates q_j, and momenta p_j, and we have assumed a bilinear system-bath coupling with coupling coefficients C_{ij} between the ith VdP oscillator and the jth harmonic oscillator of the bath. From Eq. (2), we can obtain an EOM for q_j,

$$m_j \ddot{q}_j + m_j \nu_j^2 q_j + \sum_i C_{ij} x_i = 0. \tag{3}$$

As for the EOMs for open VdP oscillators, we note that the system-bath Hamiltonians in Eq. (2) will add a linear force $-\sum_j C_{ij} q_j$ to the original nonlinear EOM for isolated counterparts, yielding

$$\ddot{x}_i + \epsilon_i \big(x_i^2 - 1\big) \dot{x}_i + \omega_i^2 x_i + F_\alpha + \sum_j C_{ij} q_j = 0. \tag{4}$$

Here F_α denotes an inherent coupling between isolated VdP oscillators, ϵ_i decides the strength of VdP nonlinearity, and ω_i represents the natural frequency of the self-sustained oscillator. We remark that one cannot assign a Hamiltonian to isolated VdP oscillators as they are inherently dissipative systems. To eliminate bath coordinates in Eq. (4), we solve Eq. (3) via the Laplace transformation,

$$\tilde{q}_j(s) = -\sum_i \frac{C_{ij}}{m_j} \frac{1}{s^2 + \nu_j^2} \tilde{x}_i(s) + I[q_j(0), \dot{q}_j(0)], \tag{5}$$

where the second term $I[q_j(0), \dot{q}_j(0)]$ on the right-hand side reflects initial conditions. We transform the above solution to the time domain and insert it into Eq. (4), and get a Langevin-type EOM for coordinate x_i of ith VdP oscillator

$$\ddot{x}_i + \epsilon_i \big(x_i^2 - 1\big) \dot{x}_i + \omega_i^2 x_i + F_\alpha + \sum_{k=1,2,\dots,N} \int_{-\infty}^{t} dt' \gamma_{ik}(t - t') \dot{x}_k(t') = \xi_i(t). \tag{6}$$

Here $\xi_i(t)$ marks a noise term experienced by the ith VdP oscillator, and $\gamma_{ik}(t - t')$ denotes a damping kernel whose explicit time dependence reflects the memory effect of baths.

They are connected via the following relations:

$$\langle \xi_i(t)\xi_k(t')\rangle = \pi T \gamma_{ik}(t-t'), \tag{7}$$

$$\gamma_{ik}(t-t') = \frac{2}{\pi}\int d\omega \frac{I_{ik}(\omega)}{\omega}\cos[\omega(t-t')] \tag{8}$$

with bath spectral functions [41,42]

$$I_{ik}(\omega) = \frac{\pi}{2}\sum_j \frac{C_{ij}C_{kj}}{m_j \nu_j^2}\delta(\omega-\nu_j), \tag{9}$$

which is a matrix element of an $N \times N$ matrix $\mathbf{I}(\omega)$. Hereafter, we refer to $\xi_i(t)$ as white noise when $\langle \xi_i(t)\xi_k(t')\rangle \propto \delta(t-t')$ (Dirac δ function) and colored otherwise.

In comparison with Eq. (1), Eq. (6) depicts several features that are worth mentioning: (1) the manner of getting Eq. (6) is semiphenomenological in the sense that we incorporated effects of baths using their Hamiltonians, (2) the external damping strength $\gamma_{\rm ext}$ in Eq. (1) is replaced by a time-dependent damping kernel $\gamma_{ik}(t-t')$, thus enabling the inclusion of effects of colored noise, (3) the bath establishes a dissipative coupling between VdP oscillators through a convolution term that plays a vital role in shaping synchronization behaviors of open VdP oscillators as we will show in the following, and (4) the noise variance is directly related to the damping kernel, as a manifestation of fluctuation-dissipation theorem. Equation (1) is recovered when the damping kernel $\gamma_{ik}(t-t') = \gamma_{\rm ext}\delta_{ik}\delta(t-t')/\pi$ and $D = T\gamma_{\rm ext}$.

B. Model description

To demonstrate the capability of the so-obtained general EOM Eq. (6), we consider a model system consisting of two coupled VdP oscillators immersed in a common thermal bath. In this scenario, the bath spectral function Eq. (9) reduces to a symmetric 2×2 matrix:

$$\mathbf{I}(\omega) = \begin{pmatrix} C_{1j}^2 & C_{1j}C_{2j} \\ C_{1j}C_{2j} & C_{2j}^2 \end{pmatrix}\frac{\pi}{2}\sum_j \frac{1}{m_j\nu_j^2}\delta(\omega-\nu_j). \tag{10}$$

We assume $C_{1j} = -C_{2j}$ such that the above equation reduces to

$$\mathbf{I}(\omega) = \begin{pmatrix} 1 & -1 \\ -1 & 1 \end{pmatrix} I(\omega) \tag{11}$$

with $I(\omega) = \sum_j \pi C_j^2\delta(\omega-\nu_j)/2m_j\nu_j^2$ a scalar spectral function. For demonstration purposes, in the present study we will consider two types of spectral function $I(\omega)$, Ohmic and Lorentzian, with the generated noise being white and colored, respectively. The damping kernels then become $\gamma_{11} = \gamma_{22} = \gamma(t-t')$, $\gamma_{12} = \gamma_{21} = -\gamma(t-t')$, with

$$\gamma(t-t') = \frac{2}{\pi}\int d\omega I(\omega)\cos[\omega(t-t')]/\omega. \tag{12}$$

Denoting $F_\gamma^i \equiv \sum_k \int_{-\infty}^t dt' \gamma_{ik}(t-t')\dot{x}_k(t')$, we find

$$F_\gamma^1 = -F_\gamma^2 \equiv F_\gamma(\dot{x}_1, \dot{x}_2) \tag{13}$$

with

$$F_\gamma(\dot{x}_1,\dot{x}_2) = \int_{-\infty}^t dt'\gamma(t-t')[\dot{x}_1(t') - \dot{x}_2(t')]. \tag{14}$$

We note that the above expression has the desired form of a dissipative velocity coupling [3] that is shown to play a crucial role in establishing synchronization [40,43]. We emphasize that our approach is not limited to the special assumption of $C_{1j} = -C_{2j}$; see Appendix A for results with $C_{1j} = C_{2j}$.

Inserting Eq. (14) into Eq. (6), the EOMs for two coupled VdP oscillators in a bath are

$$\ddot{x}_1 + \epsilon(x_1^2 - 1)\dot{x}_1 + \omega_1^2 x_1 + F_\alpha = -F_\gamma + \xi(t), \tag{15}$$

$$\ddot{x}_2 + \epsilon(x_2^2 - 1)\dot{x}_2 + \omega_2^2 x_2 - F_\alpha = F_\gamma - \xi(t). \tag{16}$$

Here ω_1 and ω_2 are natural frequencies of isolated VdP oscillators that can be nonequal. The parameter ϵ controls the VdP nonlinearity [2,19]. F_α stands for intrinsic direct coupling interaction, taking a usual conservative elastic form $F_\alpha = \alpha(x_1 - x_2)$. We have denoted the noise terms $\xi_1(t) = -\xi_2(t) = \xi(t)$ in accordance with signs of damping kernels. The above two coupled EOMs will be solved using second-order stochastic Runge-Kutta algorithms [44–46].

III. THERMAL BATH WITH OHMIC SPECTRUM

We first consider a bath with an Ohmic spectrum $I(\omega) = \gamma_{\rm ext}\omega$ [see Eq. (11)] that generates a Gaussian white noise,

$$\gamma(t-t') = 2\gamma_{\rm ext}\delta(t-t'), \quad \langle \xi(t)\xi(t')\rangle = 2T\gamma_{\rm ext}\delta(t-t'). \tag{17}$$

As a result, Eq. (14) reduces to $F_\gamma = \gamma_{\rm ext}(\dot{x}_1 - \dot{x}_2)$. We note that in some existing studies [18,24,31] just the value of D [cf. Eq. (1)] is tuned without considering its fine expression $D = \gamma_{\rm ext}T$ according to the fluctuation-dissipation theorem. Here we find that varying D only may not be sufficient to capture the rich dynamical behaviors in open VdP oscillators induced by the interplay between $\gamma_{\rm ext}$ and T; $\gamma_{\rm ext}$ characterizes the strength of dissipative coupling that facilitates synchronization [40,43] and T determines the randomness of thermal motion that tends to destroy synchronization.

To illustrate this point, we adopt the Lissajous figure [2] (see also Ref. [47] for a nice introduction) that can reflect whether the two VdP oscillators synchronize with respect to a single effective frequency (which are usually different from their natural ones) with a fixed phase difference. The Lissajous figure is a regular and stable closed curve formed by two oscillation signals, for example, x_1 and x_2 in our calculation, in a mutually perpendicular direction on the x-y plane. There are several characteristics for a Lissajous figure: (1) if the frequency ratio between two signals is irrational (nonsynchronized), the curve is dense on the plane, (2) if the frequency ratio is a rational number, the curve is an algebraic curve, (3) a high-order ratio corresponds to a high-order algebraic curve (such as 1:n synchronization [2]), and (4) when the frequencies of two signals are the same (synchronized), the figure depicts simple curves: ellipse, circle, and even a straight line with a fixed phase difference $\Delta\phi \in (0, \frac{\pi}{2})$ or $(\frac{\pi}{2}, \pi)$, $\Delta\phi = \pi/2$ and $\Delta\phi = 0$ or π, respectively. A set of numerical results showing Lissajous figures with a fixed $D = 0.01$ but different $\gamma_{\rm ext}$ and T is shown in Fig. 1. From Fig. 1(a) we clearly visualize an ellipse, indicating that the two VdP oscillators synchronize with respect to a single effective frequency with a fixed phase difference $\Delta\phi \in (0, \frac{\pi}{2})$ [47]. In contrast, the Lissajous figure in Fig. 1(b) depicts no sign of synchronization as the pattern reflects that the two VdP oscillators

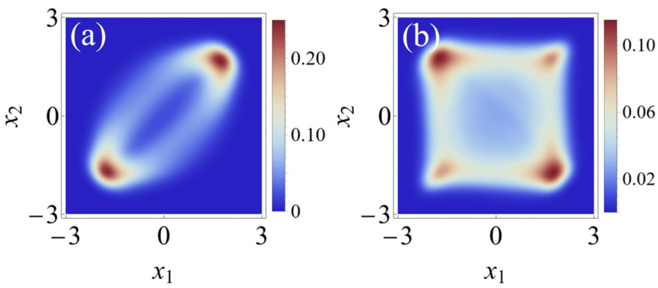

FIG. 1. Lissajous figures using an ensemble of 100 long-time trajectories. (a) $\gamma_{\rm ext} = 0.05$, $T = 0.2$; (b) $\gamma_{\rm ext} = 0.01$, $T = 1$. Other parameters are $\alpha = 0$, $\epsilon = 0.1$, $\omega_1 = 1$, and $\omega_2 = 1.03$.

do not oscillate with respect to a single frequency and the phase difference is also not fixed. Hence, it is clear that under the same value of $D = 0.01$ the system would be in either a synchronized state or a nonsynchronized one. With this in mind, in the following we will treat $\gamma_{\rm ext}$ and T separately.

A. Limit cycle under white noise

As a hallmark of self-sustainability, a stable limit cycle would be established in an isolated VdP oscillator described by Eq. (1) without the noise term ξ and the external damping $\gamma_{\rm ext}$, as a result of an intriguing balance between intrinsic energy supply and dissipation through a nonlinear term $ax^2\dot{x}$ [2]. When coupling a self-sustained oscillator to a thermal bath, one would naturally expect that such an energy balance between gain and loss in isolated VdP oscillators is broken owing to unbalanced (random) energy input and dissipation from the bath. To proceed with the study on synchronization of open VdP oscillators, it is thus important to address whether the limit cycle remains a valid notion in the presence of baths, thereby providing valuable information regarding whether synchronization can be established in open VdP oscillators.

To gain some insights into the issue, we consider a single open VdP oscillator subject to a white noise for an illustration and numerically obtain its trajectory in the phase space by solving Eq. (14) with $F_\alpha = 0$ and F_γ containing only $\dot{x}$, which may read

$$\ddot{x} + \epsilon(x^2 - 1)\dot{x} + \gamma_{\rm ext}\dot{x} + \omega_0^2 x = \xi(t). \tag{18}$$

A typical set of numerical results on trajectories in the phase space with fixed $\gamma_{\rm ext}$ and varying bath temperatures is depicted in Fig. 2. For comparison, we also present results for the limit cycle of an isolated VdP oscillator. On the single trajectory level (left column of Fig. 2), we see that the trajectory of an open VdP oscillator with a red (light gray) solid line is not closed even in the long-time limit, in stark contrast to a black closed one (which is just the limit cycle) for an isolated counterpart. As the temperature increases, the trajectory becomes more and more ergodic and deviates from the original limit cycle significantly at a high temperature, rendering the limit cycle an invalid notion. To average the randomness inherent to a single trajectory, we further plot histograms of an ensemble of 100 trajectories in the right column of Fig. 2. A smooth ring structure around the original limit cycle is clearly visualized when the temperature is relatively low. Increasing temperature will broaden the ring and finally degrade it at high temperature. Hence, we argue that one can still use the

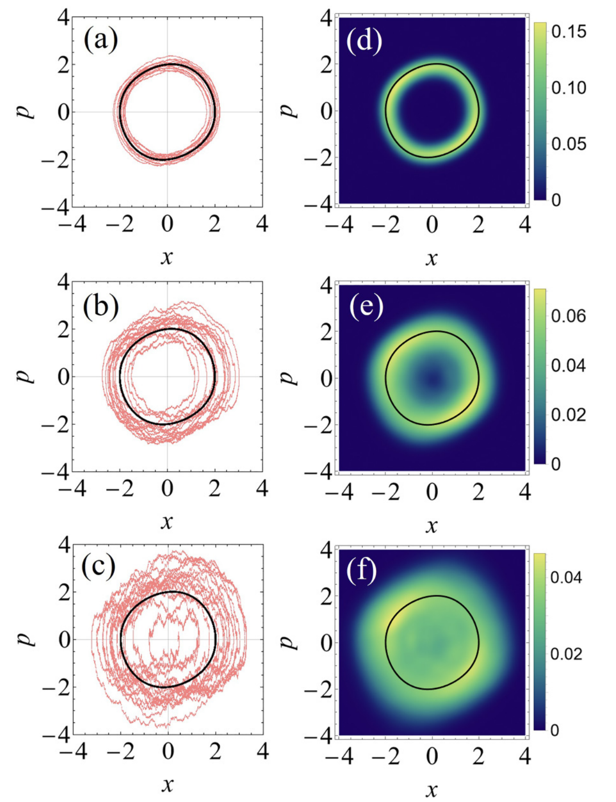

FIG. 2. Trajectory results in the phase space of a single open VdP oscillator subject to white noise with varying temperatures (a), (d) $T = 0.5$, (b), (e) $T = 5$, and (c), (f) $T = 20$. Here $p \equiv \dot{x}$ is the scaled momentum of the VdP oscillator. Left column: long-time single trajectory results as red (light gray) solid line. Right column: histograms of 100 trajectories. Black solid lines in all plots mark the corresponding limit cycle for an isolated VdP oscillator under the same oscillator parameter values. Other parameters are $\epsilon = 0.1$, $\gamma_{\rm ext} = 0.01$, and $\omega_0 = 1$.

notion of limit cycle in scenarios of open VdP oscillators at the ensemble average level provided that the temperature is not large compared with the oscillator frequency. In the following, we will limit our study to moderate temperatures.

To complement numerical results shown in Fig. 2, we follow Refs. [48,49] and adopt a generalized harmonic function transformation as $x(t) = A(t)\cos[\omega_0 t + \theta(t)]$ and $\dot{x}(t) = -A(t)\omega_0 \sin[\omega_0 t + \theta(t)]$ to perform an analytical treatment. These two trial solutions satisfy a self-consistent equation: $\dot{A}\cos[\omega_0 t + \theta(t)] = A\dot{\theta}\sin[\omega_0 t + \theta(t)]$. Inserting the above trial solutions into Eq. (18) and utilizing the self-consistent relation, we receive two coupled equations for $A(t)$ and $\theta(t)$, respectively,

$$\begin{aligned}\dot{A} &= -\epsilon A^3\cos^2\phi\sin^2\phi + (\epsilon - \gamma_{\rm ext})A\sin^2\phi - \frac{\xi(t)}{\omega_0}\sin\phi,\\ \dot{\theta} &= -\epsilon A^2\cos^3\phi\sin\phi + (\epsilon - \gamma_{\rm ext})\sin\phi\cos\phi - \frac{\xi(t)}{A\omega_0}\cos\phi.\end{aligned} \tag{19}$$

Here $\phi(t) \equiv \omega_0 t + \theta(t)$.

Generally speaking, $A(t)$ and $\theta(t)$ are stochastic functions of time. For a weak nonlinearity $\epsilon \to 0$ and a zero-mean random force $\xi(t)$ as considered here, we can employ the

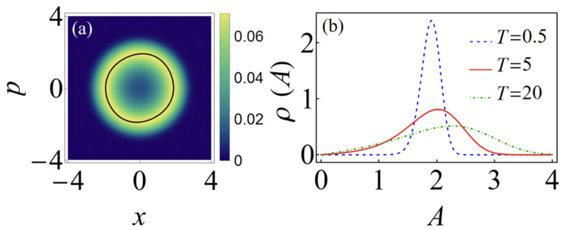

FIG. 3. (a) Phase space density $\rho(x, p)$ [Eq. (23)] with $T = 5$; (b) steady-state solution $\rho(A)$ [Eq. (22)] with varying temperature. Black solid line in (a) marks the corresponding limit cycle for an isolated VdP oscillator under the same oscillator parameter values. Other parameters are $\epsilon = 0.1$, $\gamma_{\rm ext} = 0.01$. and $\omega_0 = 1$.

Stratonovich-Khasminskii limit theorem that states that $A(t)$ and $\theta(t)$ weakly converge to a two-dimensional Markov process [50,51] after a stochastic averaging procedure. Therefore, we can introduce the following averaged stochastic representations for $A(t)$ and $\theta(t)$ in Itō forms:

$$\begin{aligned} dA &= m_1 dt + \sigma_1 dB(t), \\ d\theta &= m_2 dt + \sigma_2 dB(t). \end{aligned} \tag{20}$$

Here $B(t)$ is the standard unit Wiener process. The averaged drift coefficients $m_{1,2}$ and diffusion coefficients $b_{1,2}$ can be determined by taking a stochastic average $\langle \mathcal{O} \rangle_\phi = \frac{1}{2\pi}\int_0^{2\pi} \mathcal{O} d\phi$ [48,49] over terms in Eq. (19). We relegate detailed expressions of $m_{1,2}$ and $b_{1,2}$ to Appendix A 1.

We now consider the probability distribution function of the amplitude A that is governed by the Fokker-Planck-Kolmogorov (FPK) equation of the following form [48,49]:

$$\frac{\partial \rho(A,t)}{\partial t} = -\frac{\partial}{\partial A}[m_1\rho] + \frac{1}{2}\frac{\partial^2}{\partial A^2}[b_1\rho]. \tag{21}$$

Here $b_1 = (\sigma_1)^2$. Since we are interested in the long-time limit cycle behavior, it is enough to consider just the steady-state solution $\rho(A)$ of Eq. (21) satisfying $\partial\rho(A)/\partial t = 0$. Inserting an ansatz $\rho(A) = CA\exp[F(A)]$ with C a normalization constant into the above equation we find the steady-state probability distribution function as

$$\rho(A) = CA\exp\left[\frac{8(\epsilon - \gamma_{\rm ext})A^2 - \epsilon A^4}{\eta^2}\right]. \tag{22}$$

Here $\eta^2 = \frac{16D}{\omega_0^2}$ is proportional to the temperature T.

Hence from the expression of $\rho(A)$ one can infer that increasing the temperature will broaden $\rho(A)$, in accordance with the previous numerical finding. To see it clearly, we use the expression $A = (x^2 + \dot{x}^2/\omega_0^2)^{1/2}$ and transform $\rho(A)$ into a probability distribution function in the phase space

$$\rho(x, p \equiv \dot{x}) \equiv \left.\frac{\rho(A)}{2\pi\omega_0 A}\right|_{A=(x^2+\dot{x}^2/\omega_0^2)^{1/2}}. \tag{23}$$

In Fig. 3(a) we depict $\rho(x, p)$ calculated using Eqs. (22) and (23) with the same parameters of Fig. 2(e). We remark that there is good agreement in both the shape and magnitude between Fig. 3(a) and Fig. 2(e), thereby providing analytical evidence that the limit cycle is still preserved at a relatively low temperature. In Fig. 3(b) we further illustrate $\rho(A)$ with varying temperatures. As expected, $\rho(A)$ flattens when increasing the temperature.

B. Zero detuning

We first consider two VdP oscillators with zero detuning, namely, $\omega_1 = \omega_2 = \omega$ in Eqs. (14) and (17). In this scenario, one already knows that isolated, yet coupled, VdP oscillators could reach either an in-phase ($\Delta\phi = 0$) or an antiphase ($\Delta\phi = \pi$) synchronized state, depending on initial phase conditions [40]. In the presence of a dissipative coupling $\propto (\dot{x}_1 - \dot{x}_2)$, we note that some studies [3,39,40] have stated that the antiphase synchronized state would become unstable and even vanish. Adopting this statement, one would naturally expect that the present model under investigation will always approach an in-phase synchronized state, independent of initial phase conditions. However, as we will show later, this expectation is correct only in the low-temperature regime when further considering bath effects.

A set of numerical results confirming this expectation is depicted in Fig. 4. We particularly select an initial phase condition that would lead to an antiphase synchronization when the bath is absent. In Fig. 4(a) we present single-trajectory results for both VdP oscillators that show a smooth transition from an antiphase synchronization (emerging when $t \lesssim 1100$) to an in-phase one (emerging when $t \gtrsim 1155$). We confirm this transition by further calculating the Pearson correlation function between two trajectories $x_1(\{t_n\})$ and $x_2(\{t_n\})$ with $\{t_n\} = (t_1 = t, t_2, \ldots, t_N = t + \Delta t)$ [21,52,53]:

$$C(t) = \frac{\sum_{n=1}^N (x_1^n - \bar{x}_1)(x_2^n - \bar{x}_2)}{\sqrt{\sum_{n=1}^N (x_1^n - \bar{x}_1)^2 \sum_{n=1}^N (x_2^n - \bar{x}_2)^2}}. \tag{24}$$

Here $x_i^n \equiv x_i(t_n)$ and $\bar{x}_i \equiv \sum_n x_i^n/N$, we fix $\Delta t = 15$ throughout this study unless otherwise stated, and a time step $t_{n+1} - t_n = 0.001$ is chosen. $C(t) = 1$ (-1) marks an ideal in-phase (antiphase) synchronization at time t. As can be seen from Fig. 4(a), $C(t)$ (black dashed-dotted line) indeed shows a transition from ~ -0.9 to 1. The line shape of the Lissajous figure in Fig. 4(b) also confirms an in-phase synchronization in the long-time limit at the ensemble level, in accordance with results in Refs. [3,39,40]. Moreover, in Fig. 4(b), we reveal an interesting phenomenon: the larger the dissipative coupling strength $\gamma_{\rm ext}$, the shorter the time required to reach an in-phase synchronization. Here we introduce a synchronization time τ by requiring $|\bar{C}|(t \geqslant \tau) \geqslant 0.99$. We consider an averaged Pearson correlation function $\bar{C}(t)$ over an ensemble of trajectories so as to eliminate inherent fluctuations at the single trajectory level. We note that such a stable in-phase synchronization results from the form of dissipative coupling $\propto (\dot{x}_1 - \dot{x}_2)$. If one instead considers the form $\propto (\dot{x}_1 + \dot{x}_2)$, a stable antiphase synchronization that is independent of initial conditions could emerge; see details in Appendix B. In Fig. 4(c) we further analyze the behaviors of the synchronization time τ as a function of the temperature T. Intriguingly, we find the synchronization time τ is a monotonic increasing function of T in the low-temperature region, indicating that the in-phase synchronization favors rather low temperatures. In contrast, we observe an opposite

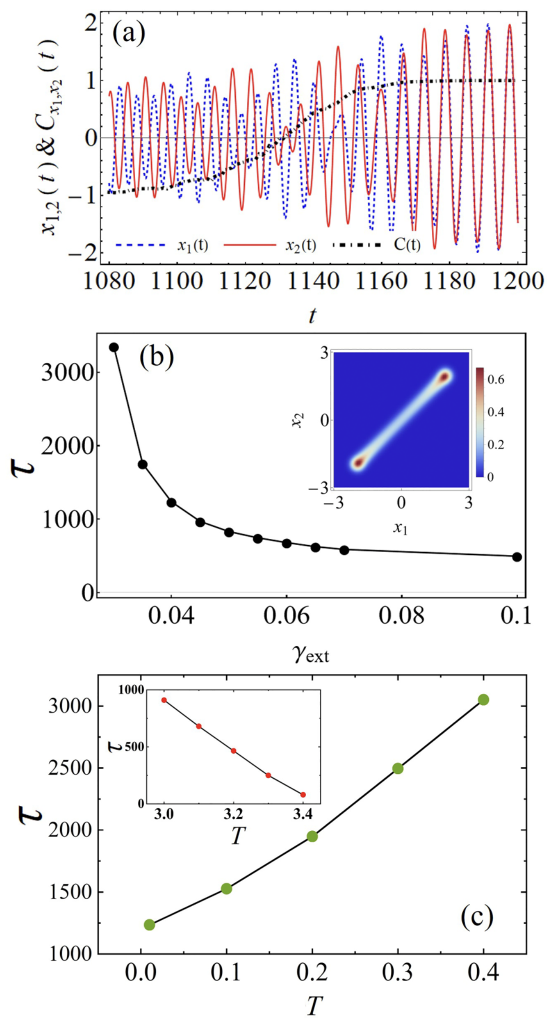

FIG. 4. Long-time in-phase synchronization in the presence of a white noise bath. (a) Time evolution of $x_1(t)$ (blue dashed line), $x_2(t)$ (red solid line), and their Pearson correlation function $C(t)$ (black dashed-dotted line) [cf. Eq. (24)] with a fixed $\gamma_{\mathrm{ext}} = 0.04$ and $T = 0.01$. (b) Synchronization time τ obtained by requiring an averaged $|\bar{C}|(t \geqslant \tau) \geqslant 0.99$ as a function of γ_{ext} with fixed $T = 0.01$. The inset shows the corresponding Lissajous figure over an ensemble at $\gamma_{\mathrm{ext}} = 0.04$. (c) Synchronization time τ as a function of temperature T in the low-temperature region with fixed $\gamma_{\mathrm{ext}} = 0.04$. The inset shows the high-temperature scenario. Other parameters are $\alpha = 0.25$, $\epsilon = 0.1$, and $\omega_0 = 1$. We selected an initial condition which would instead lead to an antiphase synchronization without the bath.

dependence of τ on T in the high-temperature region as can be seen from the inset of Fig. 4(c).

Complementing the studies [3,39,40], we find that increasing temperature would turn a stable in-phase synchronization to a stable antiphase one as illustrated in Fig. 5. At an intermediate temperature value [Fig. 5(a)], a transition behavior could be observed from the Lissajous pattern that is depicted as a mixture of line shapes with slopes 1 and -1, corresponding to a fixed phase difference $\Delta\phi = 0$ (in-phase) and π (antiphase), respectively. We can then infer that as the temperature increases from $T = 0.01$ (cf. Fig. 4) to $T = 1$ [cf. Fig. 5(a)] a noticeable part of the trajectory pairs $\{x_1(\{t_n\}), x_2(\{t_n\})\}$ es-

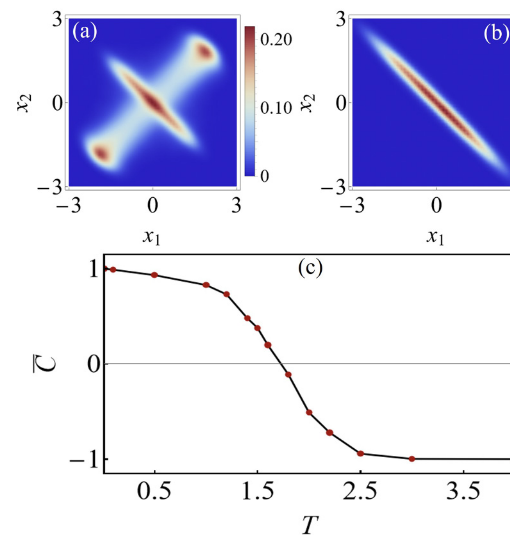

FIG. 5. (a), (b) Lissajous figure on $x_1 - x_2$ using an ensemble of 100 long-time trajectories with varying temperatures (a) $T = 1$ and (b) $T = 4$. (c) Long-time Pearson correlation function $\bar{C}$ averaged over an ensemble of 500 trajectories as a function of temperature T. Other parameters and the initial phase condition are the same as in Fig. 4.

tablishes an antiphase synchronization in the long-time limit. When we further increase the temperature to $T = 4$, we can see from Fig. 5(b) that only the line shape with slope -1 survives, indicating that the system has entered into a stable antiphase synchronized state. To visualize such a transition with increasing temperature, in Fig. 5(c) we show behaviors of the long-time ensemble-averaged Pearson correlation coefficient $\bar{C}$ as a function of temperature T. From the curve, it is clear that for low temperatures ($\bar{C} > 0.9$ when $T \lesssim 0.8$) the majority of trajectories are synchronized in an in-phase manner. As the temperature increases, $\bar{C}$ drops rapidly, marking an intermediate regime where in-phase and antiphase synchronized trajectories coexist. When the temperature reaches the high-temperature regime ($\bar{C} < -0.9$ when $T \gtrsim 2.4$), the value of $\bar{C}$ indicates that most of the trajectories are synchronized in an antiphase manner. Furthermore, from the inset of Fig. 4(c), we can infer that the antiphase synchronization favors high temperatures. Noting at high temperatures that the effect of the noise term dominates, we attribute this transition to the opposite signs of the noise term $\xi(t)$ in Eqs. (15) and (16) that force the two oscillators to synchronize in an antiphase way. In Appendix B, we show that an in-phase synchronization indeed emerges at high temperatures [cf. Fig. 12(c)] when the signs of the noise term are the same [cf. Eqs. (B3) and (B4)].

C. Nonzero detuning

We then turn to VdP oscillators with unequal natural frequencies $\omega_1 \neq \omega_2$ and focus on another typical characteristic in synchronization, a frequency entrainment, which means that oscillators with different natural frequencies will tend to oscillate with the same effective frequency $\omega_{\mathrm{eff}} \neq \omega_{1,2}$ in a synchronized state. To highlight the effect of the bath, here we set $\alpha = 0$ such that the two isolated VdP oscillators cannot synchronize at all [28].

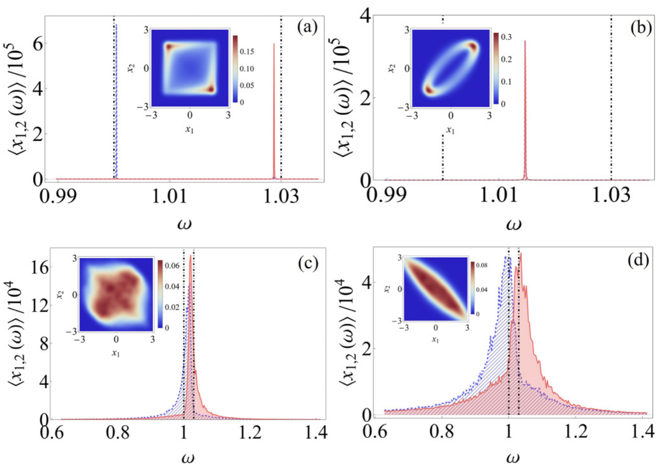

FIG. 6. Fourier spectrum $\langle x_1(\omega)\rangle$ (blue dashed line with hatched region) and $\langle x_2(\omega)\rangle$ (red solid line with shaded region) averaged over an ensemble of 500 trajectories: (a) $\gamma_{\rm ext} = 0.01$, $T = 0.1$, (b) $\gamma_{\rm ext} = 0.05$, $T = 0.1$, (c) $\gamma_{\rm ext} = 0.05$, $T = 1.5$, and (d) $\gamma_{\rm ext} = 0.05$, $T = 10$. The insets show the corresponding Lissajous figures. Other parameters are $\alpha = 0$, $\epsilon = 0.1$, and $\omega_{1(2)} = 1(1.03)$ (marked as black dashed-dotted vertical lines in both plots).

To make the frequency entrainment phenomenon visible, we analyze behaviors of $\langle x_{1,2}(\omega)\rangle$ that are Fourier transforms of averaged time-dependent displacements $\langle x_{1,2}(t)\rangle$ of oscillators over an ensemble of trajectories. A typical set of results for $\langle x_{1,2}(\omega)\rangle$ with varying damping $\gamma_{\rm ext}$ and T is depicted in Fig. 6. We first fix the temperature T to a relatively small value and vary $\gamma_{\rm ext}$ in Figs. 6(a) and 6(b). We find that increasing $\gamma_{\rm ext}$, or equivalently, the magnitude of the dissipative coupling F_γ, would induce an in-phase synchronization as confirmed by both the frequency entrainment shown in Fig. 6(b) and a Lissajous figure in its inset. This is quite intriguing since the two isolated VdP oscillators cannot synchronize with the same system parameter values.

Next we fix $\gamma_{\rm ext}$ and vary the temperature T as shown in Figs. 6(b), 6(c), and 6(d). From the comparison between them, it is evident that increasing temperature will broaden the spectrum and shift the peaks towards opposite directions. We note that a similar phenomenon was observed in Kramers oscillators [18]. Interestingly, although the frequency entrainment is completely suppressed by thermal noise at high temperatures as can be seen from Fig. 6(d), the corresponding Lissajous figure shown in the inset of Fig. 6(d) suggests an antiphase synchronization occurs with just the phase locked, unlike the in-phase synchronization that emerges at low temperatures [cf. Fig. 6(b)] with both the frequency and phase locked. To complement results in Fig. 6, we calculate the Pearson correlation function $C(t)$ as illustrated in Fig. 7(a). The results confirm the existence of a nonideal in-phase (antiphase) synchronization with $C(t) \sim 0.8\ (-0.8)$ at low (high) temperatures. Hence, similar to the zero-detuning scenario analyzed before, here increasing the temperature would also result in a transition from an in-phase synchronization to an antiphase one. As for the synchronization time τ in scenarios with nonzero detunings, we have numerically checked that its behavior as a function of temperature is similar to that shown in Fig. 4(c).

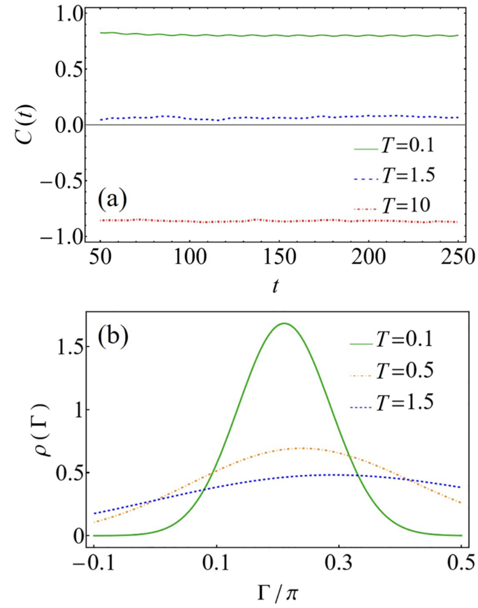

FIG. 7. (a) Pearson correlation function $\bar{C}(t)$ averaged over an ensemble of 500 trajectories with varying temperature: $T = 0.1$ (green solid line), $T = 1.5$ (blue dashed line), and $T = 10$ (red dashed-dotted line). (b) The probability distribution function $\rho(\Gamma)$ [Eq. (30)] with $A = 2$ and varying temperature: $T = 0.1$ (green solid line), $T = 0.5$ (orange dashed-dotted line), and $T = 1.5$ (blue dashed line). Other parameters are the same as in Fig. 6.

D. Coupled oscillators: An analytical treatment

To gain a better understanding of numerical results for coupled oscillators, we utilize the stochastic averaging method [50,51] to solve coupled EOMs (15) and (16). For simplicity, we assume the absence of an intrinsic coupling, namely, $F_\alpha = 0$. Similar to the analytical treatment displayed in Sec. III B, we can introduce trial solutions $x_i(t) = A_i(t)\cos\phi_i(t)$ and $\dot{x}_i(t) = -A_i(t)\omega_i \sin\phi_i(t)$, where $\phi_i(t) = \omega_i t + \theta_i(t)$ and $i = 1, 2$ [54]. Self-consistent relations $\dot{A}_i \cos\phi_i(t) = A_i\dot{\theta}_i \sin\phi_i(t)$ are imposed. Inserting the trial solutions into Eqs. (15) and (16), one can derive four equations for $\dot{A}_i$ and $\dot{\theta}_i$ (see Appendix A 2), which will weakly converge to a four-dimensional diffusive Markov process [54,55]. Further taking into account the fact that coupled oscillators can exhibit internal resonance when $\Delta = |\omega_1 - \omega_2| \to 0$, we introduce a variable $\Gamma = \phi_1 - \phi_2$, representing the phase difference between coupled oscillators. Γ is slowly varying near resonance [2] even though ϕ_i changes rapidly.

Taking a stochastic averaging with $\langle \mathcal{O}\rangle_{\phi_1} = \frac{1}{2\pi}\int_0^{2\pi} \mathcal{O} d\phi_1$ [50,51] over the equations for $\dot{A}_i$ and $\dot{\theta}_i$, we get three Itō-type equations [55]:

$$\begin{aligned} dA_1 &= m_1^c dt + \sigma_1^c dB(t), \\ dA_2 &= m_2^c dt + \sigma_2^c dB(t), \\ d\Gamma &= m_3^c dt + \sigma_3^c dB(t), \end{aligned} \tag{25}$$

where $B(t)$ is a standard unit Wiener process by noting that the two oscillators are immersed in the same thermal bath. We relegate detailed expressions for drift coefficients $m^c_{1,2,3}$ and diffusion coefficients $\sigma^c_{1,2,3}$ (the superscript "c" reflects the coupled scenario) to Appendix A 2. Then we can obtain the FPK equation describing the probability distribution $\rho(A_1, A_2, \Gamma, t)$:

$$\frac{\partial\rho}{\partial t} = \sum_{i,j=1}^{2}\left(-\frac{\partial}{\partial A_i}[m^c_i\rho] + \frac{1}{2}\frac{\partial^2}{\partial A_i\partial A_j}[b_{ij}\rho] + \frac{\partial^2}{\partial A_i\partial\Gamma}[b_{i3}\rho]\right) - \frac{\partial}{\partial\Gamma}[m^c_3\rho] + \frac{1}{2}\frac{\partial^2}{\partial\Gamma^2}[b_{33}\rho]. \tag{26}$$

Here $i, j = 1, 2$ and $b_{nm} \equiv \sigma^c_n\sigma^c_m$ $(n, m = 1, 2, 3)$. We still consider the steady-state solution $\rho(A_1, A_2, \Gamma)$ satisfying $\partial\rho(A_1, A_2, \Gamma)/\partial t = 0$. For weakly coupled systems, one can neglect the dependence of probability distribution on amplitudes $A_{1,2}$ [2,7]. Under this simplification, one just needs to consider the probability distribution function $\rho(\Gamma)$ that satisfies the following simplified FPK equation:

$$\frac{1}{2}\frac{\partial}{\partial\Gamma}[b_{33}(\Gamma)\rho(\Gamma)] - m^c_3(\Gamma)\rho(\Gamma) = 0. \tag{27}$$

First, we consider the limit of $D = 0$ where the system dynamics becomes deterministic. In this limit, $b_{33}(\Gamma) = 0$ [see Eq. (A9)], we have $m^c_3(\Gamma) = 0$ from Eq. (27), which yields the following condition [see Eq. (A6)]:

$$\Delta - \frac{\gamma_{\rm ext}}{2}\left(\frac{A_2\omega_2}{A_1\omega_1} + \frac{A_1\omega_1}{A_2\omega_2}\right)\sin\Gamma \approx \Delta - \gamma_{\rm ext}\sin\Gamma = 0. \tag{28}$$

Here we have utilized the phase reduction approximation $A_1\omega_1 \approx A_2\omega_2$ at a small detuning [7]. Interestingly, we find that Eq. (28) has the form of the Adler equation $\dot{\Theta} = \Delta - \gamma\sin\Theta = 0$ in the steady-state limit [2]. Solutions of Eq. (28) exist only when the dissipative coupling strength $\gamma_{\rm ext} > \Delta$, otherwise a steady-state synchronization could never occur. With this requirement and increasing $\gamma_{\rm ext}$ gradually, we easily deduce from Eq. (28) that the phase difference $\Gamma = \arcsin(\Delta/\gamma_{\rm ext})$ tends to vanish, indicating that the system favors an in-phase synchronization. In this regard, a special case is the zero detuning scenario with $\Delta = 0$, which always leads to $\Gamma = 0$ regardless of the value of $\gamma_{\rm ext}$. Hence the Adler equation [cf. Eq. (28)] captures the influence of dissipative coupling strength on synchronization, corroborating the conclusions presented in Secs. III B and III C.

Then we move to the low-temperature regime with $D \neq 0$. Adopting an ansatz $\rho(\Gamma) = C' \cdot e^{[-\lambda(\Gamma)]}$ with C' a normalization constant and inserting it into Eq. (27) we can get the following equation:

$$b_{33}(\Gamma)\frac{\partial\lambda(\Gamma)}{\partial\Gamma} = -\frac{2D\sin\Gamma}{A_1A_2\omega_1\omega_2} - 2m^c_3(\Gamma), \tag{29}$$

from which we find the stationary probability distribution function

$$\rho(\Gamma) = C'\exp\left[\frac{-2A\Delta(1+\Delta)\tan(\Gamma/2)}{\gamma_{\rm ext}T}\right] \times[\cos(\Gamma/2)]^{A[A(1+\Delta)^2-T]/T}. \tag{30}$$

In the low-temperature regime, we note that the amplitude of an isolated deterministic VdP oscillator $A \to 2$ [7].

In Fig. 7(b) we illustrate $\rho(\Gamma)$ with varying temperatures. At low temperatures, $\rho(\Gamma)$ depicts a relative shape peak located around a nonzero phase difference Γ_0, indicating that the coupled oscillators will reach a nonideal in-phase synchronization in the long-time limit, which is consistent with previous numerical findings. The exact value of Γ_0 can be obtained by solving $\lambda'(\Gamma_0) = 0$ using Eq. (29). In particular, when $\Delta = 0$, we can immediately get $\Gamma_0 = 0$, implying a perfect in-phase synchronization. As the temperature increases, $\rho(\Gamma)$ broadens and the phase difference is no longer fixed to a specific value. This would explain why a decrease in the long-time ensemble-averaged Pearson correlation coefficient $\bar{C}$ is observed in Fig. 7(a); see also Fig. 5(c).

From Eq. (30) we notice that when the temperature exceeds $T > A(1+\Delta)^2 \simeq 2(1+\Delta^2)$ the exponent of the cosine function becomes negative. As a result, the function $\lambda'(\Gamma)$ no longer has any zero points. Then $\rho(\Gamma)$ becomes a monotonic increasing function of Γ and diverges when $\Gamma \to \pi$, thereby indicating that the coupled oscillators form an antiphase synchronization. We remark that the critical temperature value $2(1+\Delta)^2$ [simply obtained by just looking at the term on the second line of Eq. (30)] with $\Delta = 0.03$ provides a good estimation of the transition temperature shown in Fig. 5(c).

To conclude this subsection, a few remarks regarding the present analytical treatment are in order.

First, under higher temperatures, the internal resonance between the two oscillators will be destroyed as can be seen from Fig. 6(d). In this scenario, we should adopt a stochastic averaging procedure tailored for systems without an internal resonance [55]. Since after stochastic averaging the linear dissipative coupling can be neglected in this case, we need to consider only the following two Itō-type equations for the ith oscillator:

$$\begin{aligned} dA_i &= f_i(A_i)dt + g_i dB(t), \\ d\theta_i &= \omega_i dt + h_i(A_i)dB(t). \end{aligned} \tag{31}$$

Here the drift and diffusion coefficients are $f_i(A_i) = (\epsilon - \gamma_{\rm ext})A_i/2 - \epsilon A_i^3/8 + D/(2\omega_i^2A_i^2)$, $g_i^2 = D/\omega_i^2$ and $h_i(A_i) = D/(\omega_i^2A_i^2)$. Note that the above equations for the two oscillators are correlated due to the same Wiener process $B(t)$. As the signs of noise terms in Eqs. (15) and (16) are opposite, one can easily find from these equations that $A_1 \approx -\omega_2A_2/\omega_1$ and $\phi_1 \approx \phi_2$. Recalling $x_i = A_i\cos\phi_i$, we naturally expect $x_1 \approx -x_2$ for rather small detuning, a sign of the antiphase synchronization.

Second, one can generalize the above considerations by accounting for two independent Wiener processes $B_{1,2}(t)$ with the same strength D [54–56]. In this scenario, since the two oscillators are completely decoupled, their phase difference can take an arbitrary value in the range $[0, 2\pi]$ and the synchronization would be absent. We argue that the correlation of random forces is an important ingredient for maintaining synchronization, and the phase relationship between two oscillators determines the synchronized phase difference at high temperatures.

IV. THERMAL BATH WITH LORENTZIAN SPECTRUM

To go beyond existing studies on open VdP oscillators which considered memoryless thermal baths, we turn to a bath with a finite memory time that represents a more realistic environment [36,37,57]. For demonstration purposes, we consider a bath with a Lorentzian spectrum:

$$I(\omega) = \frac{\gamma_{\rm ext}\omega}{(\omega^2 - \Omega^2)^2 + 4\Gamma^2\omega^2}. \tag{32}$$

Here Ω and Γ are two parameters controlling the peak position and broadening of the spectrum, respectively. This spectrum leads to a colored noise $\xi(t)$ satisfying the following correlation function:

$$\langle \xi(t)\xi(t')\rangle = T\gamma(t-t'), \tag{33}$$

with the damping kernel

$$\gamma(t-t') = \frac{\gamma_{\rm ext}\tau}{4\Omega\omega'}e^{-|t-t'|/\tau}\cos(\omega'|t-t'| + \theta). \tag{34}$$

Here $\tau = 1/\Gamma$ denotes the memory time, and in the following we will consider a small Γ corresponding to a long memory time, $\omega' = \sqrt{\Omega^2 - \Gamma^2}$ is a renormalized frequency, and $\theta = \arccos(\omega'/\Omega)$. Now the dissipative coupling in Eqs. (15) and (16) takes the following form:

$$F_\gamma(\dot{x}_1, \dot{x}_2) = \frac{\gamma_{\rm ext}\tau}{4\Omega\omega'}\int_{-\infty}^{t} dt' e^{-|t-t'|/\tau} \times \cos(\omega'|t-t'| + \theta)[\dot{x}_1(t') - \dot{x}_2(t')]. \tag{35}$$

A. Limit cycle under Lorentzian noise

Similar to the white noise scenario, we would like to first address the limit cycle behavior when a VdP oscillator is immersed in a bath with a Lorentzian spectrum. In Fig. 8(a) we first consider an off-resonant case in which the peak position Ω of the Lorentzian spectrum is away from the natural frequency ω_1 of the VdP oscillator such that the influence of bath is expected to be small. As can be seen from Fig. 8(a), the open VdP oscillator has almost the same limit cycle with the isolated counterpart regardless of temperature values. When the Lorentzian spectrum is in resonance with the open VdP oscillator, namely, $\Omega = \omega_1$, the limit cycle behavior can be affected by both the broadening of the spectrum and the temperature of the bath. Comparing Fig. 8(b) with 8(a), we see that moving to the resonant condition will broaden the limit cycle as well as shift the peak position of the cycle relative to that of the isolated counterpart marked by a red solid cycle. Increasing the temperature further can restore the peak position of cycle but enlarge its broadening as can be inferred from the comparison between Figs. 8(c) and 8(b). We note that such a broadening can be suppressed by decreasing the value of Γ or equivalently, increasing the memory time. However, the shape of the limit cycle will be deformed relative to that of the isolated counterpart as can be found from Fig. 8(d). Nevertheless, we can conclude that an open VdP oscillator subject to a colored noise can still permit the existence of a limit cycle even under a resonant condition.

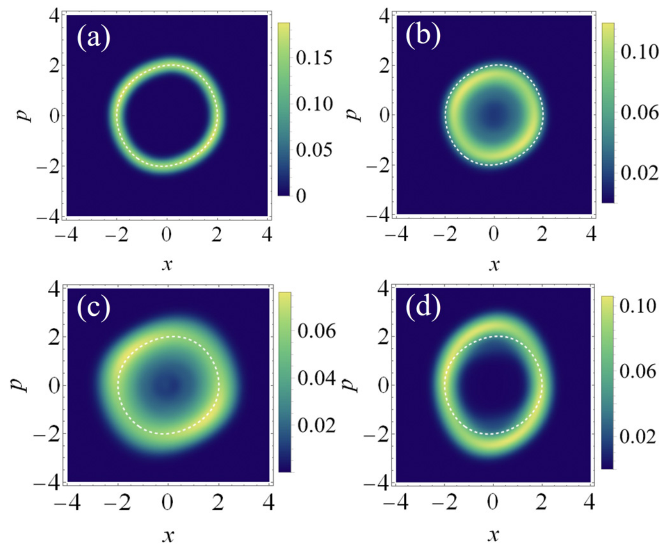

FIG. 8. Histograms of 100 trajectories in the phase space of a single open VdP oscillator subject to Lorentz colored noise. Off-resonant case: (a) $\Omega = 2$, $\Gamma = 0.025$, and $T = 0.5$. Resonant cases: (b) $\Omega = 1$, $\Gamma = 0.025$, and $T = 0.5$; (c) $\Omega = 1$, $\Gamma = 0.025$, and $T = 5$; and (d) $\Omega = 1$, $\Gamma = 0.005$, and $T = 5$. White dashed circles in all plots mark the corresponding limit cycle for an isolated VdP oscillator under the same oscillator parameter values. Other parameters are $\epsilon = 0.1$, $\gamma_{\rm ext} = 2\times 10^{-4}$, and $\omega_1 = 1$.

B. Low-temperature bath

First, we focus on a low-temperature regime with $T = 0.1$ where the bath-induced dissipative coupling plays a major role. We exemplify the effect of the bath-induced dissipative coupling in a system with nonzero detuning $\omega_1 \neq \omega_2$ by noting that an isolated counterpart cannot establish synchronization. We illustrate a bath-induced synchronization phenomenon in Fig. 9 by varying the damping strength $\gamma_{\rm ext}$. At a small $\gamma_{\rm ext}$, there is no synchronization of two open VdP oscillators as can be inferred from the Lissajous figure shown in Fig. 9(a) as well as an oscillating Pearson correlation function $C(t)$ (blue dashed line) depicted in Fig. 9(c). Increasing $\gamma_{\rm ext}$ by an order of magnitude, we see from Fig. 9(b) that a nearly in-phase synchronization can be established between two open VdP oscillators, which is further confirmed by a Pearson correlation function $C(t) \simeq 1$ (red solid line) in the long-time limit as illustrated in Fig. 9(c). We note that the observed behavior in the low-temperature regime is quite similar to that (cf. Fig. 4) in the white noise scenario.

We further look at the effects of the central frequency Ω and broadening Γ of the Lorentzian spectrum on synchronization. For simplicity, we focus on behaviors of the averaged Pearson correlation function $C(t)$ [cf. Eq. (24)]. In Fig. 10(a) we fix Γ and vary Ω; noting that we have two oscillators with $\omega_1 \neq \omega_2$, an ideal resonant case with $\Omega = \omega_{1,2}$ does not exist. Nevertheless, when Ω is close to both $\omega_{1,2}$, we can obtain a Pearson correlation function $C(t) \to 1$ in the long-time limit as can be inferred from the blue dashed line with $\Omega = 1.01$. Once Ω deviates from $\omega_{1,2}$, the long-time value of the Pearson correction function $C(t)$ is reduced (red dotted-dashed line with $\Omega = 1.35$) and becomes even an oscillating function when the deviation $|\Omega - \omega_{1,2}|$ is significantly large. In

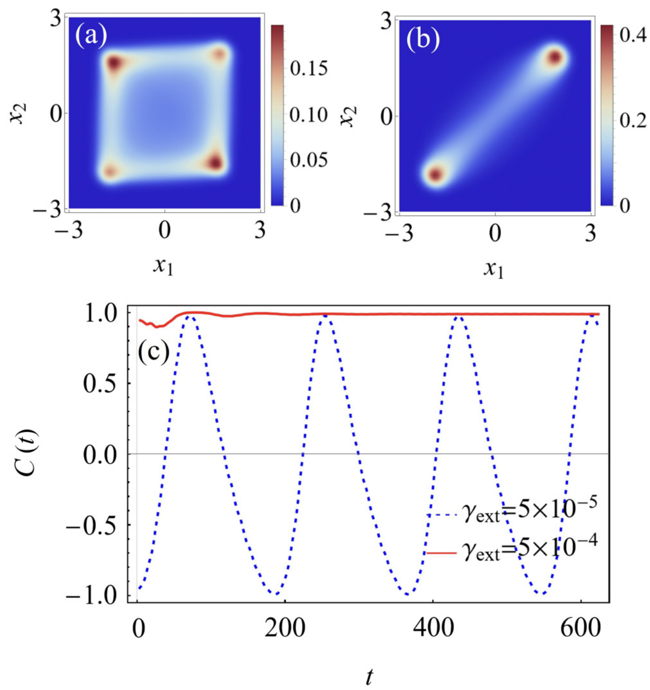

FIG. 9. Long-time in-phase synchronization in the presence of a Lorentz low-temperature bath. Lissajous figure on $x_1 - x_2$ in the long-time limit with different dissipative coupling strength (a) $\gamma_{\mathrm{ext}} = 5 \times 10^{-5}$ and (b) $\gamma_{\mathrm{ext}} = 5 \times 10^{-4}$. (c) Pearson correlation function $C(t)$ [cf. Eq. (24)] with $\gamma_{\mathrm{ext}} = 5 \times 10^{-5}$ (blue dashed line) and $\gamma_{\mathrm{ext}} = 5 \times 10^{-4}$ (red solid line). An ensemble of 500 trajectories is used for average. Other parameters are $T = 0.1$, $\Gamma = 0.025$, $\Omega = 1.01$, $\epsilon = 0.1$, and $\omega_{1(2)} = 1(1.03)$.

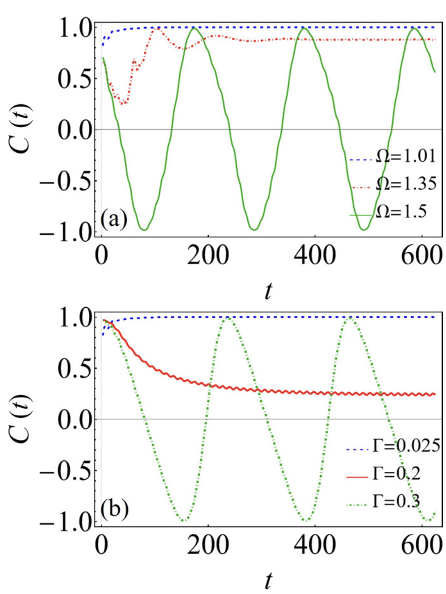

FIG. 10. Pearson correlation function $C(t)$ with (a) $\Gamma = 0.025$ and varying central frequency $\Omega = 1.01$ (blue dashed line), $\Omega = 1.35$ (red dashed-dotted line), and $\Omega = 1.5$ (green solid line). (b) $\Omega = 1.01$ and varying $\Gamma = 0.025$ (blue dashed line), $\Gamma = 0.2$ (red solid line), and $\Gamma = 0.3$ (green dashed-dotted line). An ensemble of 500 trajectories is used for average. Other parameters are $T = 0.1$, $\gamma_{\mathrm{ext}} = 5 \times 10^{-3}$, $\epsilon = 0.1$, and $\omega_{1(2)} = 1(1.03)$.

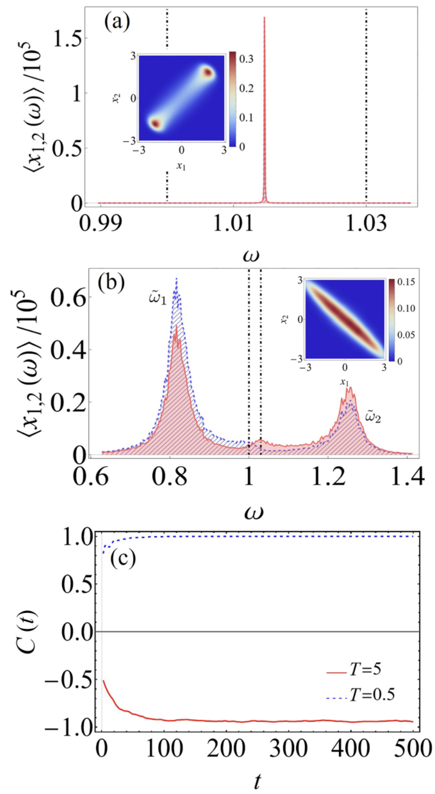

FIG. 11. Effect of temperature in the long-time limit: Fourier spectrum $\langle x_1[\omega]\rangle$ (blue dashed line with hatched region) and $\langle x_2[\omega]\rangle$ (red solid line with shaded region) with (a) $T = 0.5$ and (b) $T = 5$. Insets: Lissajous figure on $x_1 - x_2$. (c) Pearson correlation function $C(t)$ with $T = 0.5$ (blue dashed line) and $T = 5$ (red solid line). An ensemble of 500 trajectories is used for average. Other parameters are $\Omega = 1.01$, $\Gamma = 0.025$, $\gamma_{\mathrm{ext}} = 5 \times 10^{-3}$, $\epsilon = 0.1$, and $\omega_{1(2)} = 1(1.03)$ [marked by vertical black dashed-dotted lines in (a) and (b)].

Fig. 10(b) we instead fix Ω and vary Γ. From the results shown in Fig. 10(b) it is evident that we should choose a long memory time ($=1/\Gamma$) in order to have a stable yet large Pearson correlation function $C(t)$ in the long-time limit; namely, the establishment of synchronization prefers long memory time.

C. High-temperature bath

We then turn to a high-temperature regime in which the effect of random thermal noise becomes dominant. Similar to the white noise scenario (cf. Fig. 5), here we also find that increasing the temperature would turn an in-phase synchronization to an antiphase one. In Figs. 11(a) and 11(b) we show Lissajous figures under an intermediate and a high-temperature value, respectively. It is evident that the Lissajous pattern changes from a straight line with slope 1 (marking an in-phase synchronization) to one with slope -1 (marking an antiphase synchronization) when increasing the temperature. We highlight this transition by further showing the averaged Pearson correlation function $C(t)$ in Fig. 11(e): Increasing the temperature, the long-time value of $C(t)$ changes from 1 to -1.

Although the transition behaviors are quite similar, we remark that the emergent antiphase synchronization in the colored noise scenario is distinct from that in the white noise counterpart in the sense of a strong frequency renormalization as revealed by the Fourier spectra $\langle x_{1,2}(\omega)\rangle$ [recall that they are Fourier transforms of $\langle x_{1,2}(t)\rangle$]. As can be seen from Fig. 11(d), the two spectra $\langle x_{1,2}(\omega)\rangle$ overlap around two new peaks with frequencies $\tilde{\omega}_{1,2} \neq \omega_{1,2}$. We attribute the appearance of these two new peaks to the interaction between VdP oscillators and the bath with a finite memory time. Noting $\omega_{1,2} \approx \Omega \approx 1$, from the EOMs one can find that the renormalized frequencies should be $\tilde{\omega}_{1,2}^2 \approx 1 + 2\lambda^2 \mp 2\sqrt{\lambda^2 + \lambda^4}$, where we have defined a constant as $\lambda^2 = \gamma_{\rm ext}/4\Omega^2\Gamma$ (see details in Appendix B). Using the parameters in Fig. 11, we get $\tilde{\omega}_1 \approx 0.814$ and $\tilde{\omega}_2 \approx 1.258$, which agree well with the two peak positions shown in Fig. 11(d). As for the low-temperature regime, one still observes a perfect frequency entrainment in Fig. 11(c), similar to the white noise scenario [cf. Fig. 6(b)].

V. SUMMARY

In this work we studied synchronization of open VdP oscillators in a common thermal bath. To enable descriptions for baths with an arbitrary memory time, we proposed a general Langevin equation obtained from the combination of an intrinsic nonlinear EOM for VdP oscillators and a Hamiltonian description for bath and oscillator-bath coupling. The obtained Langevin equation revealed that the bath can induce a dissipative coupling between VdP oscillators, besides the usual noise and damping terms connected by the fluctuation-dissipation theorem.

To demonstrate the utility of the general Langevin equation as well as uncover the effects of a common thermal bath on synchronization behavior, we consider a setup consisting of two VdP oscillators coupled to a bath with either an Ohmic or a Lorentzian spectrum, corresponding to a white or colored noise scenario, respectively. Though the memory time of bath varies, we identify several common features regarding the synchronization behavior in open VdP oscillators: First, we revealed that the limit cycle which represents a long-time periodic motion for isolated VdP oscillators remains a valid notion at the ensemble-average level for open VdP counterparts provided that the bath temperature is moderate. Second, we found that a thermal bath is able to fix the long-time synchronization type to be either in-phase or antiphase, a phenomenon that occurs regardless of initial conditions and is sensitive only to bath temperatures. Third, we showed that a thermal bath can induce synchronization of open VdP oscillators whose isolated counterparts cannot be synchronized, owing to the presence of a bath-induced dissipative coupling. We expect that the so-obtained general Langevin equation and the way to derive it can be easily extended to other self-sustained systems, thereby promoting the studies of environmental effects on synchronization behaviors.

ACKNOWLEDGMENTS

D.R. and C.W. acknowledge the financial support from the National Key Research and Development Program of China (Grant No. 2017YFA0303104). J.L. acknowledges support from the National Natural Science Foundation of China (Grant No. 12205179), Shanghai Pujiang Program (Grant No. 22PJ1403900), and start-up funding of Shanghai University.

APPENDIX A: AVERAGED DRIFT AND DIFFUSION COEFFICIENTS

1. A single oscillator

The averaged drift and diffusion coefficients involved in Eq. (20) could be obtained directly from Eqs. (19):

$$\begin{aligned} m_1 &= \frac{1}{2\pi}\int_0^{2\pi}[-\epsilon A^3\cos^2\phi\sin^2\phi + (\epsilon-\gamma_{\rm ext})A\sin^2\phi]d\phi \\ &\quad + \frac{1}{2\pi}\int_0^{2\pi}\frac{D}{A\omega_0^2}\cos^2\phi d\phi \\ &= -\frac{1}{8}\epsilon A^3 + \frac{1}{2}(\epsilon-\gamma_{\rm ext})A + \frac{D}{2A\omega_0^2}, \end{aligned} \tag{A1}$$

$$b_1 = (\sigma_1)^2 = \frac{1}{2\pi}\int_0^{2\pi}\frac{2D}{\omega_0^2}\sin^2\phi d\phi = \frac{D}{\omega_0^2}. \tag{A2}$$

We remark that the term on the right-hand-side of the second line of Eq. (A1) corresponds to the Wong-Zakai correction term [50], which can be understood as the expectation value of a white noise. Similarly, we could get $m_2 = 0$ and $b_2 = (\sigma_2)^2 = D/A^2\omega_0^2$.

2. Coupled oscillators

The averaged drift and diffusion coefficients involved in Eqs. (25) and (26) can be obtained by first writing four first-order differential equations for A_i and θ_i:

$$\begin{aligned} \dot{A}_1 &= -\epsilon A_1^3\cos^2\phi_1\sin^2\phi_1 + (\epsilon-\gamma_{\rm ext})A_1\sin^2\phi_1 \\ &\quad + \gamma_{\rm ext}A_2\frac{\omega_2}{\omega_1}\sin\phi_1\sin\phi_2 - \frac{\xi(t)}{\omega_1}\sin\phi_1, \\ \dot{A}_2 &= -\epsilon A_2^3\cos^2\phi_2\sin^2\phi_2 + (\epsilon-\gamma_{\rm ext})A_2\sin^2\phi_2 \\ &\quad + \gamma_{\rm ext}A_1\frac{\omega_1}{\omega_2}\sin\phi_1\sin\phi_2 + \frac{\xi(t)}{\omega_2}\sin\phi_2, \\ \dot{\theta}_1 &= -\epsilon A_1^2\cos^3\phi_1\sin\phi_1 + (\epsilon-\gamma_{\rm ext})\sin\phi_1\cos\phi_1 \\ &\quad + \gamma_{\rm ext}\frac{A_2\omega_2}{A_1\omega_1}\sin\phi_2\cos\phi_1 - \frac{\xi(t)}{A_1\omega_1}\cos\phi_1, \\ \dot{\theta}_2 &= -\epsilon A_2^2\cos^3\phi_2\sin\phi_2 + (\epsilon-\gamma_{\rm ext})\sin\phi_2\cos\phi_2 \\ &\quad + \gamma_{\rm ext}\frac{A_1\omega_1}{A_2\omega_2}\sin\phi_1\cos\phi_2 + \frac{\xi(t)}{A_2\omega_2}\cos\phi_2. \end{aligned} \tag{A3}$$

Next, we determine the drift and diffusion coefficients by performing a stochastic average over equations in Eq. (A3). The detailed expressions for the drift coefficients $m_{1,2,3}^c$ are

$$\begin{aligned} m_1^c &= \frac{1}{2\pi}\int_0^{2\pi}\bigg[-\epsilon A_1^3\cos^2\phi_1\sin^2\phi_1 + (\epsilon-\gamma_{\rm ext})A_1\sin^2\phi_1 \\ &\quad + \frac{D}{A_1\omega_1^2}\cos^2\phi_1 + \gamma_{\rm ext}\frac{A_2\omega_2}{\omega_1}\sin\phi_1\sin(\phi_1-\Gamma)\bigg]d\phi_1 \\ &= -\frac{1}{8}\epsilon A_1^3 + \frac{1}{2}(\epsilon-\gamma_{\rm ext})A_1 + \gamma_{\rm ext}\frac{A_2\omega_2}{2\omega_1}\cos\Gamma + \frac{D}{2A_1\omega_1^2}, \end{aligned} \tag{A4}$$

$$m_2^c = \frac{1}{2\pi}\int_0^{2\pi}\bigg[-\epsilon A_2^3\cos^2(\phi_1-\Gamma)\sin^2(\phi_1-\Gamma) + (\epsilon-\gamma_{\rm ext})A_2\sin^2(\phi_1-\Gamma) + \frac{D}{A_2\omega_2^2}\cos^2(\phi_1-\Gamma) + \gamma_{\rm ext}\frac{A_1\omega_1}{\omega_2}\sin\phi_1\sin(\phi_1-\Gamma)\bigg]d\phi_1$$
$$= -\frac{1}{8}\epsilon A_2^3 + \frac{1}{2}(\epsilon-\gamma_{\rm ext})A_2 + \gamma_{\rm ext}\frac{A_1\omega_1}{2\omega_2}\cos\Gamma + \frac{D}{2A_2\omega_2^2}, \tag{A5}$$

$$m_3^c = \Delta + \frac{\gamma_{\rm ext}}{2\pi}\int_0^{2\pi}\bigg[\frac{A_2\omega_2}{A_1\omega_1}\sin(\phi_1-\Gamma)\cos\phi_1 - \frac{A_1\omega_1}{A_2\omega_2}\sin\phi_1\cos(\phi_1-\Gamma)\bigg]d\phi_1$$
$$= \Delta - \frac{\gamma_{\rm ext}}{2}\left(\frac{A_2\omega_2}{A_1\omega_1} + \frac{A_1\omega_1}{A_2\omega_2}\right)\sin\Gamma. \tag{A6}$$

The detailed expressions for the diffusion coefficients $\sigma^c_{1,2,3}$ are

$$b_{11} = (\sigma_1^c)^2 = \frac{1}{2\pi}\int_0^{2\pi}\frac{2D}{\omega_1^2}\sin^2\phi_1 d\phi_1 = \frac{D}{\omega_1^2}, \tag{A7}$$

$$b_{22} = (\sigma_2^c)^2 = \frac{1}{2\pi}\int_0^{2\pi}\frac{2D}{\omega_2^2}\sin^2(\phi_1-\Gamma) d\phi_1 = \frac{D}{\omega_2^2}, \tag{A8}$$

$$b_{33} = (\sigma_3^c)^2 = \frac{2D}{2\pi}\int_0^{2\pi}\left[\frac{\cos\phi_1}{A_1\omega_1} + \frac{\cos(\phi_1-\Gamma)}{A_2\omega_2}\right]^2 d\phi_1$$
$$= \frac{D}{A_1^2\omega_1^2} + \frac{D}{A_2^2\omega_2^2} + \frac{2D\cos\Gamma}{A_1A_2\omega_1\omega_2}, \tag{A9}$$

$$b_{12} = \sigma_1^c\sigma_2^c = \frac{2D}{2\pi}\frac{1}{\omega_1\omega_2}\int_0^{2\pi}\sin\phi_1\sin(\phi_1-\Gamma)d\phi_1$$
$$= -\frac{D}{\omega_1\omega_2}\cos\Gamma = b_{21}, \tag{A10}$$

$$b_{13} = \sigma_1^c\sigma_3^c = \frac{2D}{2\pi}\frac{1}{A_2\omega_1\omega_2}\int_0^{2\pi}\sin\phi_1\cos(\phi_1-\Gamma)d\phi_1$$
$$= \frac{D}{A_2\omega_1\omega_2}\sin\Gamma = b_{31}, \tag{A11}$$

$$b_{23} = \sigma_2^c\sigma_3^c = \frac{2D}{2\pi}\frac{1}{A_1\omega_1\omega_2}\int_0^{2\pi}\sin(\phi_1-\Gamma)\cos\phi_1 d\phi_1$$
$$= \frac{D}{A_1\omega_1\omega_2}\sin\Gamma = b_{32}. \tag{A12}$$

Using Eqs. (A4)–(A12), the FPK equation (26) is thus completely determined.

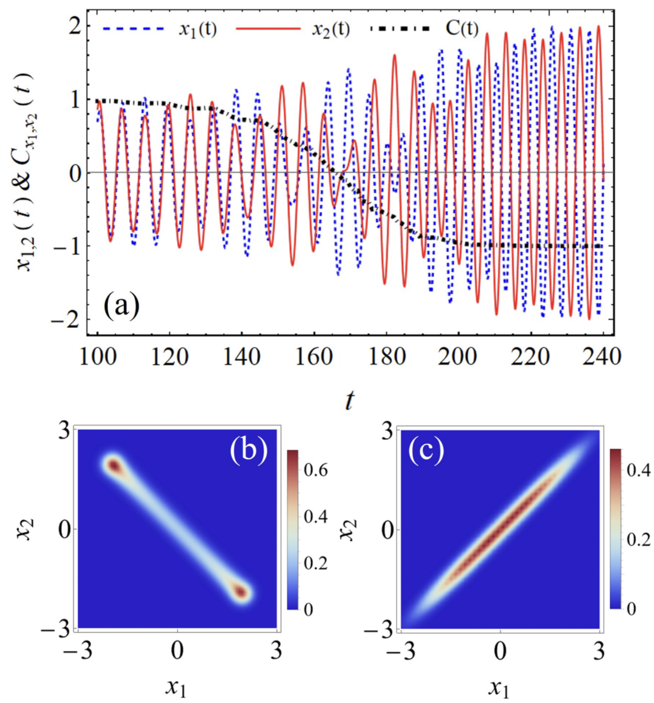

FIG. 12. Synchronization behaviors obtained from Eqs. (B3) and (B4). (a) Single-trajectory results of $x_1(t)$ (blue dashed line), $x_2(t)$ (red solid line), and their Pearson correlation function $C(t)$ (black dashed-dotted line) [cf. Eq. (24)] with a fixed $\gamma_{\rm ext} = 0.04$ and temperature $T = 0.01$. (b, c) Lissajous figure on x_1-x_2 averaged over an ensemble of 300 trajectories in the long-time limit with fixed $\gamma_{\rm ext} = 0.04$ and varying temperature (b) $T = 0.01$, (c) $T = 4$. Other parameters are $T = 0.01$, $\alpha = 0.25$, $\epsilon = 0.1$, and $\omega_{1,2} = 1$. We selected an initial condition that would instead lead to an in-phase synchronization without the bath.

APPENDIX B: SYNCHRONIZATION FROM A DIFFERENT COUPLING FORM

In the main text, we consider a coupling form with coupling coefficients satisfying $C_{1j} = -C_{2j}$ [cf. Eq. (10)]. In this Appendix we instead consider a scenario with $C_{1j} = C_{2j}$ so as to emphasize that our general EOM (6) holds regardless of specific relations between coupling coefficients. For simplicity, we focus on a bath with an Ohmic spectrum. Now the function $\mathbf{I}(\omega)$ in Eq. (11) is replaced by

$$\mathbf{I}(\omega) = \begin{pmatrix}1 & 1\\ 1 & 1\end{pmatrix} I(\omega), \tag{B1}$$

leading to new forms of dissipative couplings $F_\gamma^1 = F_\gamma^2 \equiv F_\gamma(\dot{x}_1, \dot{x}_2)$ with

$$F_\gamma(\dot{x}_1,\dot{x}_2) = \int_{-\infty}^t dt'\gamma(t-t')[\dot{x}_1(t') + \dot{x}_2(t')] \tag{B2}$$

as well as new EOMs governing the dynamics of $x_{1,2}(t)$:

$$\ddot{x}_1 + \epsilon(x_1^2-1)\dot{x}_1 + \omega_1^2 x_1 + F_\alpha = F_\gamma + \xi(t), \tag{B3}$$

$$\ddot{x}_2 + \epsilon(x_2^2-1)\dot{x}_2 + \omega_2^2 x_2 - F_\alpha = F_\gamma + \xi(t). \tag{B4}$$

For a zero-detuning setup at a low temperature, both the Pearson correlation function $C(t) \to -1$ shown in Fig. 12(a)

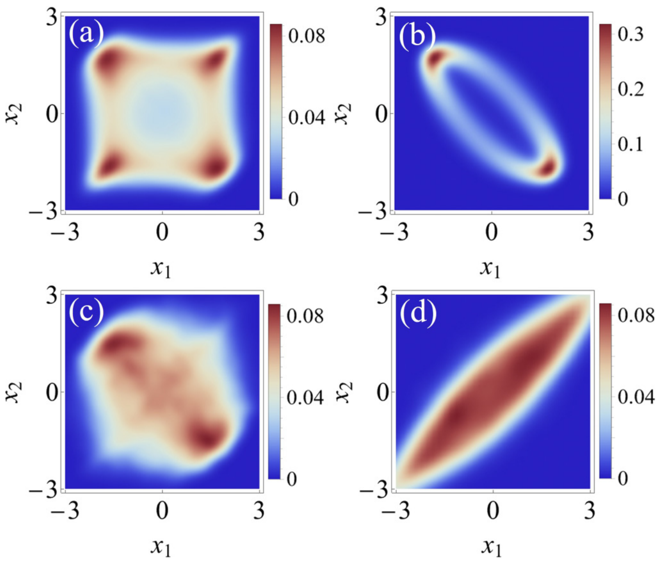

FIG. 13. Lissajous figure on x_1-x_2 averaged over an ensemble of 300 trajectories in the long-time limit from Eqs. (B3) and (B4): (a) $\gamma_{\mathrm{ext}} = 0.01$, $T = 0.1$, (b) $\gamma_{\mathrm{ext}} = 0.05$, $T = 0.1$, (c) $\gamma_{\mathrm{ext}} = 0.05$, $T = 1.5$, and (d) $\gamma_{\mathrm{ext}} = 0.05$, $T = 10$. Other parameters are $\alpha = 0$, $\epsilon = 0.1$, and $\omega_{1(2)} = 1(1.03)$.

and a line shape Lissajous pattern with slope −1 depicted in Fig. 12(b) indicate that the system is stabilized to an antiphase synchronization by the bath. Comparing with results in Figs. 4(a) and 4(c), we know that the sign reversal in the relation between C_{1j} and C_{2j} would change the fixed synchronous phase difference from 0 (in-phase synchronization) to π (antiphase synchronization). Increasing the temperature induces a transition from an antiphase synchronization to an in-phase one as can be seen from Fig. 12(c).

For a setup with a nonzero detuning, we contrast Lissajous figures in Fig. 13 with those in Fig. 6. From Fig. 13(a) and 13(b), we see that increasing damping strength would result in an antiphase synchronization at a low temperature. Increasing temperature, the Lissajous figure gradually changes from an antiphase synchronization to finally an in-phase one [Fig. 13(d)], similar to the zero-detuning scenario.

APPENDIX C: FREQUENCY RENORMALIZATION DUE TO COLORED NOISE AT HIGH TEMPERATURE

In this Appendix we show how to obtain renormalized frequencies observed in the colored noise scenario at high temperature [cf. Fig. 11(d)] from the general EOMs [cf. Eqs. (15) and (16)]. Noting that we set the intrinsic direct coupling to be zero and the nonlinear term proportional to ϵ can be neglected in the high-temperature regime, we have the following simplified EOMs from Eqs. (15) and (16):

$$\ddot{x}_1 + \omega_1^2 x_1 + F_\gamma(\dot{x}_1, \dot{x}_2) = \xi(t), \tag{C1}$$

$$\ddot{x}_2 + \omega_2^2 x_2 - F_\gamma(\dot{x}_1, \dot{x}_2) = \xi(t). \tag{C2}$$

Here $F_\gamma(\dot{x}_1, \dot{x}_2) = \int_{-\infty}^{t} dt' \gamma(t - t')[\dot{x}_1(t') - \dot{x}_2(t')]$ which, in the case of a colored noise, can be rewritten as

$$F_\gamma(\dot{x}_1, \dot{x}_2) = \int_{-\infty}^{t} dt' \dot{\gamma}(t - t')[x_1(t') - x_2(t')]. \tag{C3}$$

As will be seen later, it is this term that induces frequency renormalizations. Combining Eqs. (C1), (C2), and (C3), we are now left with linear EOMs which, in the Laplace domain, are

$$\begin{pmatrix} s^2 + \omega_1^2 + Z & -Z \\ -Z & s^2 + \omega_2^2 + Z \end{pmatrix} \begin{pmatrix} \tilde{x}_1(s) \\ \tilde{x}_2(s) \end{pmatrix} = \begin{pmatrix} \tilde{\xi}(s) \\ \tilde{\xi}(s) \end{pmatrix}. \tag{C4}$$

In arriving at the above equation, we have utilized Eq. (34). We also defined $Z \equiv 2\lambda^2 \frac{s^2 + 2\Gamma s}{s^2 + 2\Gamma s + \Omega^2}$ with $\lambda^2 = \frac{\gamma_{\mathrm{ext}}}{4\Omega^2 \Gamma}$. In the absence of thermal baths, we have $Z = 0$ such that the poles of the solutions for $\tilde{x}_{1,2}(s)$ mark the frequencies (noting the relations between Laplace and Fourier transformations). Inspired by this observation, we first make the approximations $\omega_{1,2} \approx \Omega \approx 1$ and $Z \approx 2\lambda^2 \frac{s^2}{s^2 + 1}$ by noting the parameter values used in obtaining Fig. 11, then diagonalize the matrix in the left-hand-side of Eq. (C4) and let the eigenvalues be zero so as to get the poles. The resulting nontrivial poles satisfy

$$s^2 + 1 + 4\lambda^2 \frac{s^2}{s^2 + 1} = 0, \tag{C5}$$

yielding renormalized frequencies $\tilde{\omega}_{1,2}^2 = -s^2 = 1 + 2\lambda^2 \mp 2\sqrt{\lambda^2 + \lambda^4}$, which are just the expressions shown in the main text.

[1] M. Bennett, M. F. Schatz, H. Rockwood, and K. Wiesenfeld, Proc. R. Soc. London, Ser. A **458**, 563 (2002).

[2] A. Pikovsky, M. Rosenblum, and J. Kurths, *Synchronization: A Universal Concept in Nonlinear Sciences*, Cambridge Nonlinear Science Series (Cambridge University Press, New York, 2001).

[3] D. Aronson, G. Ermentrout, and N. Kopell, Physica D **41**, 403 (1990).

[4] V. Varshney, G. Saxena, B. Biswal, and A. Prasad, Chaos **27**, 093104 (2017).

[5] H. Sakaguchi and Y. Kuramoto, Prog. Theor. Phys. **76**, 576 (1986).

[6] T. E. Lee and H. R. Sadeghpour, Phys. Rev. Lett. **111**, 234101 (2013).

[7] S. Walter, A. Nunnenkamp, and C. Bruder, Ann. Phys. **527**, 131 (2015).

[8] C.-H. Fan, L. Du, H.-X. Zhang, and J.-H. Wu, J. Phys. B **51**, 175503 (2018).

[9] C.-G. Liao, R.-X. Chen, H. Xie, M.-Y. He, and X.-M. Lin, Phys. Rev. A **99**, 033818 (2019).

[10] B. van der Pol, London Edinburgh Dublin Philos. Mag. J. Sci. **3**, 65 (1927).

[11] E. B. M. Ngouonkadi, H. B. Fotsin, and P. L. Fotso, Phys. Scr. **89**, 035201 (2014).

[12] R. G. Paccosi, A. Figliola, and J. Galán-Vioque, SIAM J. Appl. Dyn. Syst. **13**, 1152 (2014).
[13] V. Vlasov, M. Komarov, and A. Pikovsky, J. Phys. A **48**, 105101 (2015).
[14] F. Dörfler and F. Bullo, SIAM J. Appl. Dyn. Syst. **10**, 1070 (2011).
[15] S. Martineau, T. Saffold, T. T. Chang, and H. Ronellenfitsch, Phys. Rev. Lett. **128**, 098301 (2022).
[16] K. Czolczynski, P. Perlikowski, A. Stefanski, and T. Kapitaniak, Physica A **388**, 5013 (2009).
[17] V. Jovanovic and S. Koshkin, J. Sound Vib. **331**, 2887 (2012).
[18] L. Callenbach, P. Hänggi, S. J. Linz, J. A. Freund, and L. Schimansky-Geier, Phys. Rev. E **65**, 051110 (2002).
[19] H. Fotsin and S. Bowong, Chaos Solitons Fractals **27**, 822 (2006).
[20] S. Al-Khawaja, Chaos Solitons Fractals **42**, 1415 (2009).
[21] S. Siwiak-Jaszek, T. P. Le, and A. Olaya-Castro, Phys. Rev. A **102**, 032414 (2020).
[22] B. Lindner, J. Garcia-Ojalvo, A. Neiman, and L. Schimansky-Geier, Phys. Rep. **392**, 321 (2004).
[23] D. S. Goldobin and A. Pikovsky, Phys. Rev. E **71**, 045201(R) (2005).
[24] J. M. Casado, J. Gómez-Ordóñez, and M. Morillo, Europhys. Lett. **79**, 50002 (2007).
[25] B. Shulgin, A. Neiman, and V. Anishchenko, Phys. Rev. Lett. **75**, 4157 (1995).
[26] J. Casado-Pascual, J. Gómez-Ordóñez, M. Morillo, J. Lehmann, I. Goychuk, and P. Hänggi, Phys. Rev. E **71**, 011101 (2005).
[27] V. V. Semenov, Phys. Rev. E **95**, 052205 (2017).
[28] S. Astakhov, A. Feoktistov, V. S. Anishchenko, and J. Kurths, Chaos **21**, 047513 (2011).
[29] K. Park, Y.-C. Lai, S. Krishnamoorthy, and A. Kandangath, Chaos **17**, 013105 (2007).
[30] Y. Song and T. A. Witten, Phys. Rev. E **106**, 044207 (2022).
[31] E. Pankratova and V. Belykh, Eur. Phys. J. Spec. Top. **222**, 2509 (2013).
[32] S. Barbay, G. Giacomelli, S. Lepri, and A. Zavatta, Phys. Rev. E **68**, 020101(R) (2003).
[33] S. H. Simpson, Y. Arita, K. Dholakia, and P. Zemánek, Phys. Rev. A **104**, 043518 (2021).
[34] M. G. Rosenblum, A. S. Pikovsky, and J. Kurths, in *The Random and Fluctuating World: Celebrating Two Decades of Fluctuation and Noise Letters* edited by P. V. E. McClintock and L. B. Kish (World Scientific, Singapore, 2022), pp. 335–344.
[35] R. Belousov, F. Berger, and A. J. Hudspeth, Phys. Rev. E **102**, 032209 (2020).
[36] B. C. Bag, S. K. Banik, and D. S. Ray, Phys. Rev. E **64**, 026110 (2001).
[37] Y.-F. Guo and J.-G. Tan, Physica A **419**, 691 (2015).
[38] A. O. Caldeira and A. J. Leggett, Physica A **121**, 587 (1983).
[39] T. Chakraborty and R. H. Rand, Int. J. Non Linear Mech. **23**, 369 (1988).
[40] M. Ivanchenko, G. Osipov, V. Shalfeev, and J. Kurths, Physica D **189**, 8 (2004).
[41] N. Freitas and J. P. Paz, Phys. Rev. E **90**, 042128 (2014).
[42] E. A. Martinez and J. P. Paz, Phys. Rev. Lett. **110**, 130406 (2013).
[43] D. W. Storti and P. G. Reinhall, in *Nonlinear Dynamics*, The Richard Rand 50th Anniversary Volume, edited by A. Guran (World Scientific, Singapore, 1997), pp. 1–23.
[44] R. Mannella and V. Palleschi, Phys. Rev. A **40**, 3381 (1989).
[45] K. Burrage, I. Lenane, and G. Lythe, SIAM J. Sci. Comput. **29**, 245 (2007).
[46] A. F. N. Rasedee, M. H. A. Sathar, H. M. Ijam, K. I. Othman, N. Ishak, and S. R. Hamzah, *Proceedings of the 3rd International Conference on Applied Science and Technology (ICAST'18)*, AIP Conf. Proc. No. 2016 (AIP, New York, 2018), p. 020120.
[47] T. B. Greenslade, Phys. Teach. **31**, 364 (1993).
[48] J. Roberts and P. Spanos, Int. J. Non Linear Mech. **21**, 111 (1986).
[49] Z. Xu and Y. Cheung, J. Sound Vib. **174**, 563 (1994).
[50] H. J. Kushner, *Approximation and Weak Convergence Methods for Random Processes, with Applications to Stochastic Systems Theory* (MIT Press, Cambridge, MA, 1984).
[51] R. Z. Khas'minskii, Theory Probab. Appl. **11**, 390 (1966).
[52] G. Karpat, İ. Yalçınkaya, and B. Çakmak, Phys. Rev. A **101**, 042121 (2020).
[53] G. L. Giorgi, F. Plastina, G. Francica, and R. Zambrini, Phys. Rev. A **88**, 042115 (2013).
[54] Y. Wu, Y. Gao, and L. Zhang, Eur. J. Mech. A-Solid **39**, 60 (2013).
[55] Y. Wu, Mech. Syst. Signal Process. **118**, 767 (2019).
[56] Z. G. Nicolaou, M. Sebek, I. Z. Kiss, and A. E. Motter, Phys. Rev. Lett. **125**, 094101 (2020).
[57] B. C. Bag, Phys. Rev. E **65**, 046118 (2002).